Functionally Modified Cellulose Nanocrystals as an Adsorbent for Anionic Dyes

Ming Li, ShiYu Fu*

State Key Laboratory of Pulp and Paper Engineering, South China University of Technology, Guangzhou, Guangdong Province, 510640*, China*

Abstract: Cellulose nanocrystal was modified with poly(N,N-diethylaminomethyl methacrylate) to prepare an adsorbent containing amine groups for removing anionic dyes from waste water. The prepared adsorbent was characterized by Fourier-transform infrared spectrometry (FT-IR), X-ray photoelectron spectroscopy (XPS), and thermogravimetric analysis (TGA). The adsorption was affected by various factors, such as the contact time, adsorbent dosage, dye solution pH value, initial dye concentration, and ionic strength. The results revealed that amine functional groups mainly contribute to the adsorption of azo dyes (AO7). The adsorbent showed pseudo-second-order adsorption kinetics, indicating that the dye molecules were chemisorbed on the adsorbent. The adsorption isotherm was found to fit better with the Langmuir isotherm model than with the Freundlich isotherm model.

Keywords: cellulose nanocrystal; anionic dye; adsorption kinetic; adsorption isotherm



Ming Li, PhD candidate;
E-mail: li163ming@163.com



*Corresponding author:
ShiYu Fu, professor, PhD tutor; research interests: pulping chemistry and nanocellulose materials;
E-mail: shyfu@scut.edu.cn

1 Introduction

Water contamination due to the discharge of dyes into water bodies has grown drastically over the past few years. Dye waste water contains a large amount of toxic azo dyes. Azo dye molecules in dye waste water are decomposed into aromatic amines and aromatic derivatives. These aromatic compounds have long been identified as carcinogenic and mutagenic and caused grievous injury to aquatic organisms and human life[1-2]. Therefore, it is essential to remove azo dyes from dye waste water before discharging it into water bodies.

Many physical/chemical methods such as coagulation/flocculation[3], anion exchange[4-5], chemical precipitation[6], electrochemical processes[7], membrane technology[8], and adsorption processes[9] have been reported for removing azo dyes from waste water. However, some of these methods are not efficient for practical

Received: 4 July 2018; accepted: 2 August 2018.

applications; for example, the electrochemical and membrane methods are expensive, while the coagulation/flocculation, precipitation, and oxidation processes produce large amounts of toxic sludge, causing secondary pollutant that need further treatment. The adsorption process is one of the most common and effective methods used to remove dyes from dye waste water. Adsorbents play the most important role in the adsorption process. Many materials such as activated carbon[2], chitosan[10], and cellulose[11] can be used as adsorbents via functional modification. Some modified materials possessing functional groups such as carboxylic[3], amine[11], and amidoxime[12] can be used as adsorbents for the removal of harmful ions from aqueous solutions. These functional groups promote both physical and chemical adsorption, and hence improve the adsorption efficiency of adsorbents. Recently, the application of grafted materials for dye adsorption has received considerable attention[1,8-10]. Zhou et al[13] synthesized ethylenediamine-modified magnetic chitosan nanoparticles via a complex route for removing AO7 from aqueous solutions. Kiransan et al prepared modified montmorillonite containing quaternary ammonium groups using cetyltrimethylammonium bromide[14]. Noorimotlagh et al[2] prepared active nano-porous carbon from milk vetch by a complex process. This carbon has nano-sized pore structure, and the pore size of 67% of the pores in the carbon is less than 100 nm. Unfortunately, the disadvantage of these adsorbent materials is that their preparation processes are very complicated and expensive. High-cost and stringent preparation conditions encounter significant challenges for widespread application of dye adsorbents. Hence, it is imperative to develop simple and cost-effective method to synthesize adsorbents for dye waste water treatment.

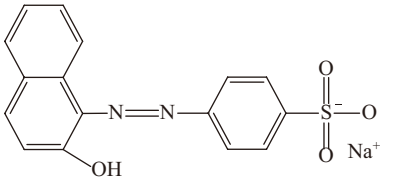
Cellulose Nanocrystal (CNC) is the most commonly used natural polymer material and possesses a large amount of active hydroxyl groups. Hence, functional monomers can be easily grafted onto it to synthesize multifunctional materials. N,N-diethylaminomethyl methacrylate (DMAEMA) is a tertiary amine-containing acrylic monomer that can be easily polymerized by various reactions such as Atom Transfer Radical Polymerization (ATRP)[15] and Reversible Addition-Fragmentation Chain Transfer Polymerization (RAFT)[16]. In this work, DMAEMA was polymerized on the surface of CNC by ATRP. The functionalized CNC was used as an adsorbent for acid orange 7 (AO7) dye. The modified CNC was characterized by Fourier transform infrared spectroscopy (FT-IR), X-ray photoelectron spectroscopy (XPS), and thermogravimetric analysis (TGA). Furthermore, the adsorption behavior of the CNC adsorbent was investigated under equilibrium and dynamic conditions.

2 Materials and methods

2.1 Chemicals and instrument

2-Bromoisobutyryl bromide (BIBB), N-methyl-2-pyrrolidone (NMP), CuBr (99%, Energy Chemical), 2-(Dimethyl amino) pyridine (DMAP), AO7, N, N, N′, N″, N″-pentamethyl diethylenetriamine (PMDETA), and 2-(diethylamino) ethylmethacrylate (DMAEMA, 99%) were purchased from Shanghai Aladdin Co., Ltd., China. N,N-dimethylformamide (DMF) and triethylamine (TEA, AR) were obtained from Tianjin Chemical Company, Tianjin, China. The chemical structure and characteristics of AO7 are shown in Table 1. DMF was dried by molecular sieves (4 Å) before use. CuBr was purified by acetic acid and ethanol. CNC was prepared using a method reported by us previously[17].

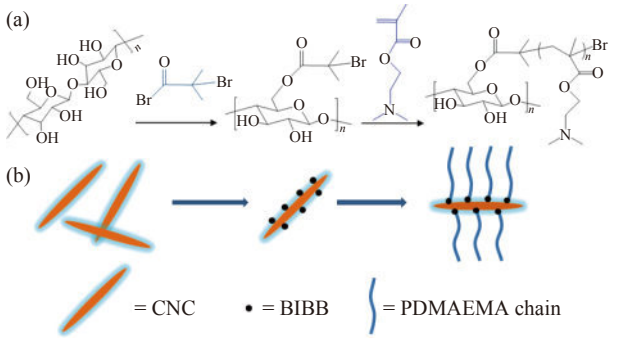
Table 1 General characteristics of AO7

Items	Parameters	Structure
Molecular formula	$C_{16}H_{11}N_2O_4SNa$	
C.I. name	Acid orange II	
Chromophore	Monoazo	
Ionization	Acidic	
Molecular weight/(g · mol^{-1})	350.32	
λ_{max}/nm	485	

FT-IR (VERTEX 70, Bruker, Germany), XPS (Kratos Axis Ultra DLD, Kratos, England), and TGA (TA Q500, USA) were used to determine the chemical structure and the surface elemental composition of the CNC samples. An ultraviolet-visible (UV-vis) spectrophotometer (G1369C, Agilent, China) was employed to determine the concentration of dye in the dye solution.

2.2 Preparation of CNC-based adsorbent

The CNC-based adsorbent was synthesized according to a previously reported method[18]. The synthesis route, which involved the ATRP of DMAEMA on CNC, is shown in Scheme 1. First, the initiator was fixed on the surface of CNC. CNC (3.24 g), NMP (200 mL), DMAP (0.02 mol), and TEA (0.03 mol) were added in a flask filled with Ar. BIBB (0.12 mol) was added to this flask over 1 h. The reaction system was then placed in an ice-water bath for 24 h. The resulting product, CNC-Br, was thoroughly washed and freeze-dried. CNC-Br (0.4 g) was then added to a flask containing DMF (30 mL), DMAEMA (0.05 mol), CuBr (0.5 mmol), and PMDETA (0.5 mmol). The polymerization reaction was carried out at 60℃ for 6 h under stirring after executing three freeze-evacuate-thaw cycles. The white product so obtained was thoroughly washed and extracted with a mixture of water and ethanol (water∶ethanol=1∶1 (*V*/*V*)) for 4 h and was finally freeze-dried.



Scheme 1 Synthesis route (a) and schematic (b) of the CNC-based adsorbent

2.3 Adsorption experiment

Batch experiments were conducted to investigate the effects of the contact time, dye solution temperature, ionic strength, initial pH value, and adsorbent dosage on the adsorption capacity of the adsorbent. A certain amount of adsorbent was added to the dye solution under stirring at 400 r/min for a predetermined time and was then removed by centrifugation. The residual concentration of AO7 in the dye solution after the adsorption was determined at 485 nm using a UV-vis spectrophotometer. The residual dye concentration was determined from a standard curve derived from a series of dye solutions with a known dye content. The adsorbent dosage in the AO7 dye (400 mg/L) solution was varied from 10 mg to 80 mg and the solution temperature was maintained at 20℃. The effect of the initial pH value on the dye removal efficiency of the adsorbent was investigated by varying the initial pH value (which was adjusted with 0.1 mol/L HCl or NaOH at the beginning) of the solution. In order to investigate the effects of the contact time and ionic strength on the adsorption of AO7 molecules onto the CNC adsorbent, different contact times (4, 8, 12, 16, 20, 30, and 40 min) and NaCl concentrations (0.001~0.1 mol/L) were used. To determine the adsorption capacity of the CNC-based adsorbent at different temperatures (i.e. 20℃ and 30℃), the initial concentration of AO7 in the adsorption medium (pH=2.0, t=20 min) was varied from 100 mg/L to 700 mg/L. All the experiments were carried out in duplicate. The dye removal efficiency of the adsorbent was calculated using Equation (1):

$$R=\frac{C_0-C_t}{C_0}\times 100\% \quad (1)$$

Where, C_0 and C_t are the concentrations (mg/L) of dye initially and at time t, respectively. The amount of dye adsorbed per unit mass of the adsorbent at equilibrium, Q_e (mg/g), was calculated using Equation (2):

$$Q_e=\frac{(C_0-C_e)\cdot V}{m} \quad (2)$$

Where, Q_e is the dye adsorbed at equilibrium, C_e is the equilibrium dye concentration (mg/L), and m and V are the mass of the adsorbent (g) and volume of the dye solution (L), respectively.

3 Results and discussion

3.1 Characterization of CNC-Br and CNC-PDMAEMA

FT-IR and XPS analyses were carried out to examine the chemical structure and surface elements of CNC-Br and CNC-PDMAEMA. BIBB was anchored on the surface of CNC by esterification to prepare the ATRP initiator. As shown in Fig.1(b), unlike CNC, CNC-Br showed a strong FT-IR peak at 1740 cm^{-1}. This peak corresponds to the stretching vibration of C═O from the ester group[19]. A strong peak at 1280 cm^{-1} corresponding to C—O was observed in the FT-IR spectrum of CNC-Br (Fig.1(b))[20]. The XPS spectrum of CNC-Br (Fig.2) showed a Br3d peak at 68 eV. It can be observed from Table 2 that the Br content in CNC-Br was 3.01%. These results suggest that BIBB was successfully grafted onto the CNC surface (reaction is shown in Scheme 1).

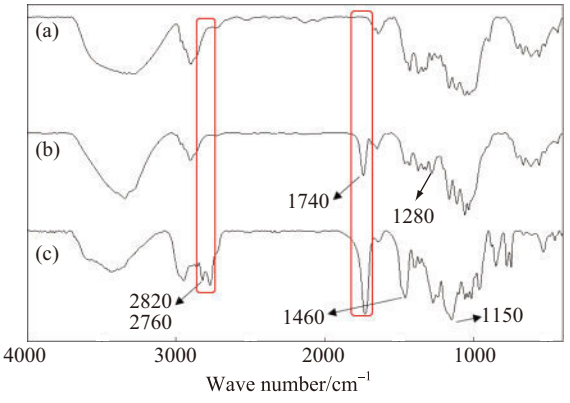


Fig.1 FT-IR spectra of (a) CNC, (b) CNC-Br, and (c) CNC-PDMAEMA

After the polymerization reaction, the intensity of the peak at 1740 cm^{-1} increased (Fig.1(b) and Fig.1(c)) because of the additional carbonyl groups from PDMAEMA. The peaks at 2946, 2822, and 2773 cm^{-1} can be attributed to the C—H groups of PDMAEMA. The peak at 1460 cm^{-1} corresponds to the C—C stretching vibration, while that at 1150 cm^{-1} corresponds to the stretching vibration of C—N from the —$N(CH_3)_2$— group. From Fig.2 it can be observed that after the polymerization, new resonance signals were generated attributing to the carbon of CNC-PDMAEMA. After the ATRP reaction of CNC-PDMAEMA, the characteristic

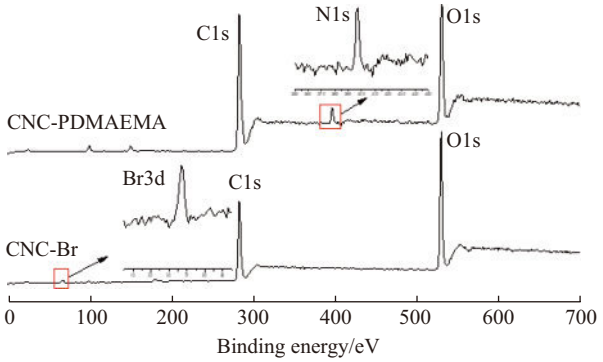


Fig.2 XPS spectra of CNC-Br and CNC-PDMAEMA

peak of N was detected at 396 eV (Fig.2). In addition, the nitrogen content in CNC-PDMAEMA increased sharply (5.03%, N1s), compared with that in CNC-Br (Table 2). These results confirm that PDMAEMA was successfully grafted onto the surface of CNC.

Table 2 Elemental surface composition of CNC–Br and CNC–PDMAEMA, as determined by XPS

Samples	Composition/%			
	C1s	O1s	N1s	Br3d
CNC-Br	53.66	43.22	0.11	3.01
CNC-PDMAEMA	67.73	25.62	5.03	0.49

The TG/differential TG (DTG) curves for CNC, CNC-Br, and CNC-PDMAEMA are shown in Fig.3. For CNC, the initial weight loss was observed at 240℃. This weight loss can be mainly attributed to the carbonization and volatilization of small molecular compounds and water[21]. The thermal decomposition of CNC-Br began at 170℃ (lower than the initial decomposition temperature of CNC) because of the release of HBr formed during the heating. The TG and DTG curves of CNC-PDMAEMA show that the weight loss occurred in three stages. In the first stage (T_1=220~290℃), almost 63% weight loss was observed because of the pyrolytic decomposition of PDMAEMA that was grafted onto CNC. In the second stage of decomposition (T_2=330℃), the weight loss occurred because of the splitting of the cellulose structure and main-chain scission. A total weight loss of about 95% was observed in the final stage (T_3=420℃) attributing to the formation of large amounts of volatile compounds and solid char from the decomposed cellulose units[22].

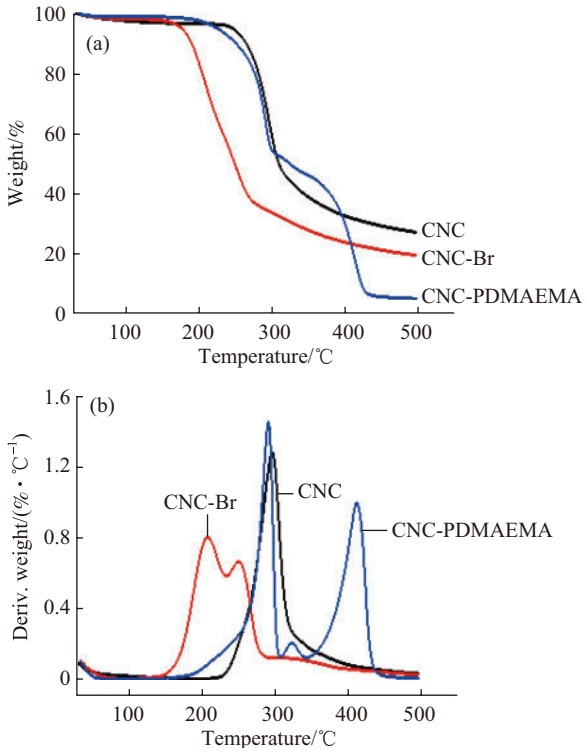


Fig.3 TG (a) and DTG (b) curves of CNC, CNC-Br, and CNC-PDMAEMA

3.2 Dye adsorption properties

3.2.1 Effects of adsorbent dosage and dye solution pH value

The dye (AO7) removal efficiency of CNC at various adsorbent dosages (10~80 mg) and dye solution pH values was measured (Fig.4). The dye removal efficiency increased with an increase in the adsorbent dosage. For a fixed initial dye concentration, an increase in the adsorbent dosage increased the adsorption area and the number of adsorption sites[2,23]. It should be noted that at the pH values of 2.0 and 4.0, an increase in the adsorbent dosage beyond 60~80 mg resulted in an insignificant increase in the AO7 removal efficiency. These results are consistent with those reported previously[2,12,24].

Moreover, it was found that AO7 removal efficiency was high under acidic conditions. This is mainly because of the pH-responsive property of PDMAEMA. The tertiary amine groups (—NR_1R_2) of PDMAEMA on the surface of CNC acted as the binding sites for anions. Under acidic conditions, these amine groups protonated to form —$NR_1R_2H^+$ groups, and the electric repulsion between the —$NR_1R_2H^+$ groups restrained the tendency of the polymer chains to collapse or aggregate in solution[19]. However, under alkaline conditions, the tertiary amine groups could not protonate and the uncharged polymer chains collapsed or aggregated. Hence, PDMAEMA grafted on the CNC adsorbent became positively charged and dissolved completely at pH=2.0 and 4.0. On the other hand, at pH=8.5, the PDMAEMA chains remained uncharged and collapsed. And acidic environment increased the number of adsorption sites and the contact area between the adsorbent and azo ions. Therefore, from Fig.4 it can be observed that the AO7 removal efficiency of the CNC-PDMAEMA adsorbent at pH=2.0 and 4.0 was far greater than that at pH=8.5 when the other conditions were the same.

3.2.2 Effect of ionic strength

The effect of ionic strength on the AO7 adsorption of CNC-PDMAEMA was investigated by carrying out dye degradation at various NaCl concentrations. As

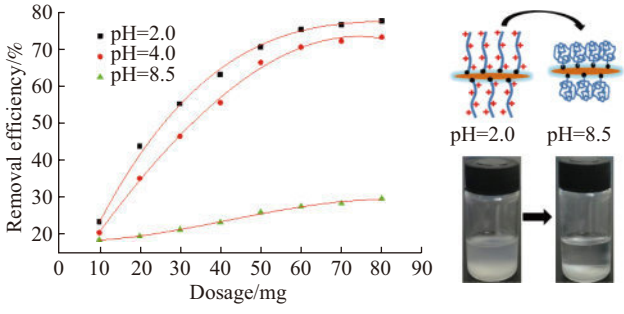


Fig.4 Effect of the adsorbent dosage on the AO7 removal efficiency of CNC-PDMAEMA at different dye solution pH values (t=20 min, T=20℃, C_0=400 mg/L)

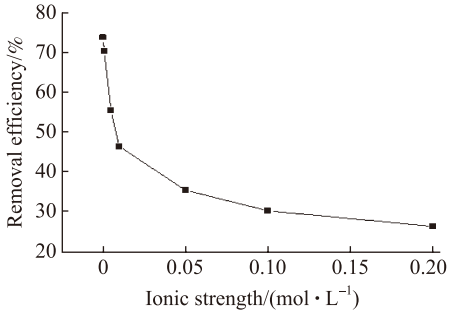


Fig.5 Effect of ionic strength (NaCl) on the AO7 removal efficiency of CNC-PDMAEMA (T=20℃, t=20 min, m_0=60 mg, C_0=400 mg/L)

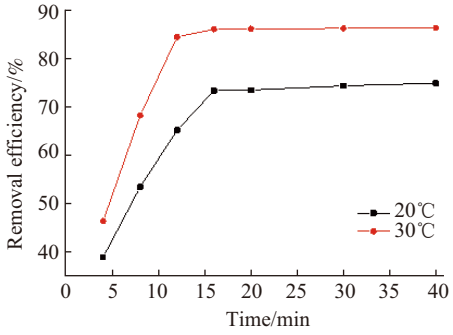


Fig.6 Effect of the contact time on the AO7 removal efficiency of CNC-PDMAEMA at different dye temperatures (m_0=60 mg, pH=2.0, C_0=400 mg/L)

can be seen from Fig.5, as the ionic strength increased from 0.001 mol/L to 0.2 mol/L, the AO7 removal efficiency decreased from 73.6% to 26.3%. This can be attributed to the competition of Cl^- with azo anions and other negative ions for adsorption sites. The presence of NaCl in high concentrations suppressed the AO7 adsorption[22].

3.2.3 *Effect of the contact time and kinetic study*

The effect of the contact time on the AO7 removal efficiency of the CNC-based adsorbent was investigated at two different temperatures (i.e. 20℃ and 30℃) and the results are shown in Fig.6. As can be seen from Fig.6, at the beginning of the adsorption, the AO7 removal efficiency increased rapidly with time. After 16 min, the adsorption process reached equilibrium. At this equilibrium, the AO7 removal efficiency did not change significantly with time. Initially, the adsorption mainly occurred on the surface of the CNC-based adsorbent. After that, the adsorption occurred on the inner surface of PDMAEMA[25], which was dominated mainly by the electrostatic interactions between azo ions and the amine groups on PDMAEMA.

Adsorption kinetics provide essential information regarding the adsorption rate and reactive pathways. Hence, we applied the pseudo first- and second-order models (most widely used kinetic models) to elucidate the adsorption process. The equations are as follows:

Pseudo-first-order: $\ln(Q_e-Q_t)=\ln Q_e-k_1 \cdot t$ (3)

Where, k_1 is the pseudo-first-order rate constant, Q_e and Q_t (mg/g) are the amounts of dye adsorbed at equilibrium and time t (min), respectively.

Pseudo-second-order: $t/Q_t=1/(k_2 \cdot Q_e^2)+t/Q_e$ (4)

Where, k_2 is the rate constant for the pseudo-second-order kinetics.

The adsorption kinetics of CNC-PDMAEMA based on the pseudo first- and second-order models are shown in Fig.7, and the estimated kinetic parameters are listed in Table 3. At the tested temperatures, the R^2 for the second-order model was >0.99, while that for the first-order model was found to be within the range 0.84~0.88. Moreover, the $Q_{e,cal}$ values (81.56 mg/g at 20℃, 89.58 mg/g at 30℃) for the pseudo-first-order model were much lower than the $Q_{e,exp}$ values (99.69 mg/g at 20℃, 114.80 mg/g at 30℃). On the other hand, the $Q_{e,cal}$ values (111.11 mg/g at 20℃, 125.00 mg/g at 30℃) for the second-order model matched well with the $Q_{e,exp}$ values. This indicates that the adsorption kinetics of CNC-PDMAEMA were better described by the pseudo-second-order model. This

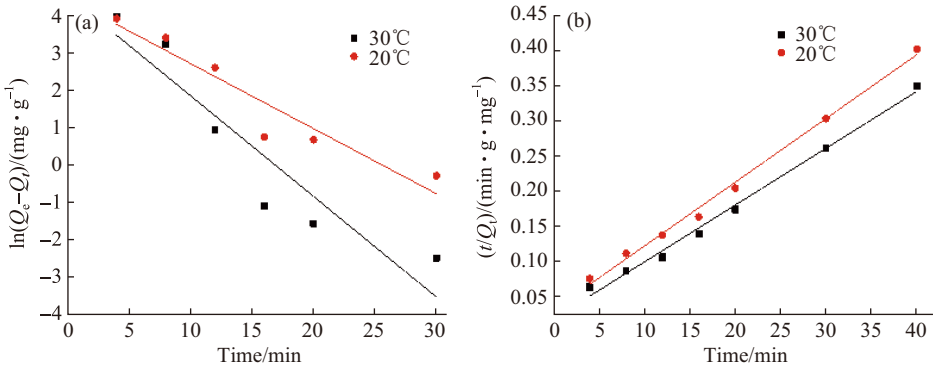


Fig.7 Pseudo-first-order adsorption rate (a) and pseudo-second-order adsorption rate (b) for the adsorption of AO7 by CNC-PDMAEMA

Table 3 Pseudo–first– and second–order parameters for the adsorption

$Q_{e,exp}$ /(mg · g^{-1})	T/℃	First-order kinetic model			Second-order kinetic model		
		$Q_{e,cal}$/(mg · g^{-1})	k_1	R^2	$Q_{e,cal}$/(mg · g^{-1})	k_2	R^2
99.69	20	81.56	0.17	0.88	111.11	2.51×10^{-3}	0.99
114.80	30	89.58	0.27	0.84	125.00	3.23×10^{-3}	0.99

suggests that the adsorption of the anionic dye onto the CNC-based adsorbent was mainly controlled by chemisorption[25-26]. The pseudo-second-order kinetics of dye adsorption have also been reported for other biomass-based materials[25, 27].

3.2.4 Effect of the initial dye concentration and adsorption isotherm

Fig.8(a) shows the effects of the initial AO7 concentration and temperature on the adsorption. The adsorption of the dye at different concentrations increased rapidly in the initial stages and decreased gradually as the adsorption progressed until the equilibrium was reached. The initial concentration provided a driving force to overcome all the mass transfer resistances (between the aqueous and solid phases) of the dye. Hence, high initial dye concentrations increased the adsorption capacity[26]. Additionally, an increase in temperature (from 20℃ to 30℃) also showed a positive effect on the adsorption. This is because the temperature increase accelerated the dye molecular diffusion rate and promoted the adsorption of AO7.

Adsorption isotherm models are used to describe the interaction between an adsorbate and adsorbent. In this study, the adsorption of AO7 onto the CNC-based adsorbent was evaluated using the Langmuir and Freundlich isotherm models. The Langmuir isotherm model, which assumes monolayer adsorption with uniform energies of adsorption on the surface, can be expressed as Equation (5):

$$C_e/Q_e=C_e/Q_m+1/(Q_m \cdot K_L) \quad (5)$$

Where, Q_e (mg/g) and C_e (mg/L) are the amounts of dye adsorbed per unit weight of biomass and dye equilibrium concentration in solution, respectively. Q_m (mg/g) denotes the monolayer adsorption capacity of the adsorbent and K_L is the Langmuir constant.

The Freundlich model is based on multilayer adsorption with the adsorption energy decreasing with the surface coverage. It is expressed as Equation (6):

$$\ln Q_e=\frac{1}{n} \cdot \ln C_e \cdot \ln K_F \quad (6)$$

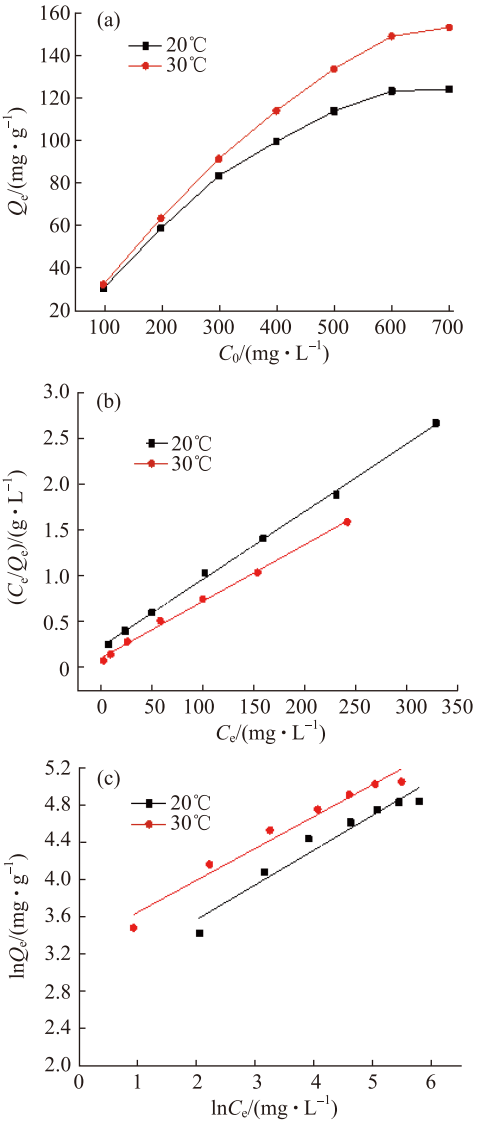


Fig.8 (a) Adsorption isotherms for the adsorption of AO7 dyes on CNC-PDMAEMA at different temperatures; (b) Linear Langmuir plot for adsorption; (c) Linear Freundlich plot for adsorption

Where, K_F is the Freundlich constant and n is an empirical parameter relating the adsorption capacity and adsorption intensity, which varies with the heterogeneity of the material.

The adsorption isotherms are shown in Fig.8(b) and Fig.8(c) and the model parameters are summarized

Table 4 Estimated kinetic parameters of the two adsorption isotherms

$Q_{e,exp}$ /(mg · g^{-1})	T/℃	Langmuir model			Freundlich model		
		K_L	$Q_{e,cal}$/(mg · g^{-1})	R^2	K_F	n	R^2
123.95	20	3.23×10^{-2}	136.43	0.99	16.78	2.70	0.94
152.93	30	5.73×10^{-2}	162.87	0.99	27.09	2.94	0.96

in Table 4. As we can see, the Langmuir isotherm model fitted the experimental data well (high correlation coefficients, R^2=0.99). The theoretical maximum adsorption capacity ($Q_{e,cal}$=136.43 mg/g at 20℃, $Q_{e,cal}$=162.87 mg/g at 30℃) matched well with the experimental values ($Q_{e,exp}$=123.95 mg/g at 20℃, $Q_{e,exp}$=152.93 mg/g at 30℃). Therefore, it can be stated that the adsorption of AO7 onto CNC-PDMAEMA showed a monolayer uniform adsorption behavior[28-29]. Moreover, the Freundlich isotherm model also described the adsorption accurately. The values of n were in the range of 1~10, indicating a favorable adsorption process[4,13,30].

4 Conclusions

In this study, we demonstrated that poly(N,N-diethylam inomethylmethacrylate) (PDMAEMA)-functionalized CNC (via ATRP) can be effectively used for removing AO7 from aqueous solutions. The CNC-PDMAEMA adsorbent was characterized by FT-IR and XPS. The results showed that the adsorbent was successfully prepared. The CNC-based adsorbent exhibited good adsorption properties. The adsorption process depended significantly on the initial pH value of the dye solution. The pH value of 2.0 favored the adsorption process. The adsorption isotherms of the CNC-PDMAEMA adsorbent could be well described by the Langmuir model, and the adsorption capacity was found to be 162.87 mg/g at 30℃. The kinetic study results showed that the adsorption process followed pseudo-second-order kinetics. Hence, CNC-PDMAEMA is a promising adsorbent for removing anionic dyes from waste water.

Acknowledgments

This work was supported by the Science and Technology Program of Guangzhou (No. 201704020038); the foundation of State Key Laboratory of Pulp and Paper Engineering (No. 2017QN01); and National Natural Science Foundation of China (No. 31570569).

References

[1] Liu Z, Zhang F, Liu T, et al. Removal of azo dye by a highly graphitized and heteroatom doped carbon derived from fish waste: adsorption equilibrium and kinetics[J]. Journal of Environmental Management, 2016, 182: 446-454.

[2] Noorimotlagh Z, Soltani R D C, Khataee A R, et al. Adsorption of a textile dye in aqueous phase using mesoporous activated carbon prepared from iranian milk vetch[J]. Journal of the Taiwan Institute of Chemical Engineers, 2014, 45(4): 1783-1791.

[3] Martínez-Quiroz M, López-Maldonado E A, Ochoa-Terán A, et al. Innovative uses of carbamoyl benzoic acids in coagulation-flocculation's processes of wastewater[J]. Chemical Engineering Journal, 2017, 307: 981-988.

[4] Greluk M, Hubicki Z. Efficient removal of acid orange 7 dye from water using the strongly basic anion exchange resin amberlite IRA-958[J]. Desalination, 2011, 278(1): 219-226.

[5] Zhai F, Wang Z, Liu Y. Preparation of lignin based anion exchanger for nitrate and phosphate removal[J]. Paper and Biomaterials, 2016, 1(1): 22-30.

[6] Petta L, De Gisi S, Casella P, et al. Evaluation of the treatability of a winery distillery (vinasse) wastewater by UASB, anoxic-aerobic UF-MBR and chemical precipitation/adsorption[J]. Journal of Environmental Management, 2017, 201: 177-189.

[7] Cotillas S, Sáez C, Cañizares P, et al. Removal of 2,4-D herbicide in soils using a combined process based on washing and adsorption electrochemically assisted[J]. Separation and Purification Technology, 2018, 194: 19-25.

[8] Vatanpour V, Salehi E, Sahebjamee N, et al. Novel chitosan/polyvinyl alcohol thin membrane adsorbents modified with detonation nanodiamonds: preparation, characterization, and adsorption performance[J]. Arabian Journal of Chemistry, 2018.

[9] Aljeboree A M, Alshirifi A N, Alkaim A F. Kinetics and equilibrium study for the adsorption of textile dyes on coconut shell activated carbon[J]. Arabian Journal of Chemistry, 2017, 10(S2): S3381-S3393.

[10] Chen Y, Ru J, Geng B, et al. Charge-functionalized and mechanically durable composite cryogels from Q-NFC and CS for highly selective removal of anionic dyes[J]. Carbohydrate Polymers, 2017, 174: 841-848.

[11] Jin L, Li W, Xu Q, et al. Amino-functionalized nanocrystalline cellulose as an adsorbent for anionic dyes[J]. Cellulose, 2015, 22(4): 2443-2456.

[12] Jin L, Sun Q, Xu Q, et al. Adsorptive removal of anionic dyes from aqueous solutions using microgel based on nanocellulose and polyvinylamine[J]. Bioresource Technology, 2015, 197: 348-355.

[13] Zhou L, Jin J, Liu Z, et al. Adsorption of acid dyes from aqueous solutions by the ethylenediamine-modified magnetic chitosan nanoparticles[J]. Journal of Hazardous

Materials, 2011, 185(2/3): 1045-1052.

[14] Kıranşan M, Soltani R D C, Hassani A, et al. Preparation of cetyltrimethylammonium bromide modified montmorillonite nanomaterial for adsorption of a textile dye[J]. Journal of the Taiwan Institute of Chemical Engineers, 2014, 45(5): 2565-2577.

[15] Wang M, Yuan J, Huang X, et al. Grafting of carboxybetaine brush onto cellulose membranes via surface-initiated ARGET-ATRP for improving blood compatibility[J]. Colloids and Surfaces B Biointerfaces, 2013, 103(1): 52-58.

[16] Roy D, Guthrie J T, Perrier S. Synthesis of natural-synthetic hybrid materials from cellulose via the raft process[J]. Soft Matter, 2008, 4: 145-155.

[17] Hu Z, Patten T, Pelton R, et al. Synergistic stabilization of emulsions and emulsion gels with water-soluble polymers and cellulose nanocrystals[J]. ACS Sustainable Chemistry & Engineering, 2015, 3: 1023-1031.

[18] Liu P, Chen Q, Wu S, et al. Surface modification of cellulose membranes with zwitterionic polymers for resistance to protein adsorption and platelet adhesion[J]. Journal of Membrane Science, 2010, 350(1): 387-394.

[19] Tang J, Lee M F, Zhang W, et al. Dual responsive pickering emulsion stabilized by poly[2-(dimethylamino) ethyl methacrylate] grafted cellulose nanocrystals[J]. Biomacromolecules, 2014, 15(8): 3052-3060.

[20] Yi, J, Xu Q, Zhang X, et al. Temperature-induced chiral nematic phase changes of suspensions of poly(N,N-dimethylaminoethyl methacrylate)-grafted cellulose nanocrystals[J]. Cellulose, 2009, 16(6): 989-997.

[21] Majoinen J, Walther A, McKee J R, et al. Polyelectrolyte brushes grafted from cellulose nanocrystals using Cu-mediated surface-initiated controlled radical polymerization[J]. Biomacromolecules, 2011, 12(8): 2997-3006.

[22] Anirudhan T S, Nima J, Divya P L. Adsorption of chromium(VI) from aqueous solutions by glycidylmethacrylate-grafted-densified cellulose with quaternary ammonium groups[J]. Applied Surface Science, 2013, 279(279): 441-449.

[23] Zhou Y, Jin Q, Zhu T, et al. Adsorption of chromium (VI) from aqueous solutions by cellulose modified with β-CD and quaternary ammonium groups[J]. Journal of Hazardous Materials, 2011, 187(1): 303-310.

[24] Kousha M, Daneshvar E, Sohrabi M S, et al. Adsorption of acid orange II dye by raw and chemically modified brown macroalga stoechospermum marginatum[J]. Chemical Engineering Journal, 2012, 192(2): 67-76.

[25] Hamzeh Y, Ashori A, Azadeh E, et al. Removal of acid orange 7 and remazol black 5 reactive dyes from aqueous solutions using a novel biosorbent[J]. Materials Science and Engineering C, 2012, 32(6): 1394-1400.

[26] Kousha M, Daneshvar E, Sohrabi M S, et al. Adsorption of acid orange II dye by raw and chemically modified brown macroalga stoechospermum marginatum[J]. Chemical Engineering Journal, 2012, 192(2): 67-76.

[27] Lin Y, Fang G G, Deng Y J. Preparation and characteristics of a pH-sensitive glucose-based hydrogel[J]. Paper and Biomaterials, 2018, 3(3): 39-46.

[28] Zhu S, Yang N, Zhang D. Poly(N,N-dimethylaminoethyl methacrylate) modification of activated carbon for copper ions removal[J]. Materials Chemistry and Physics, 2009, 113(2): 784-789.

[29] Bayramoglu G, Yakuparica M. Adsorption of Cr(VI) onto PEI immobilized acrylate-based magnetic beads: isotherms, kinetics and thermodynamics study[J]. Chemical Engineering Journal, 2008, 139(1): 20-28.

[30] Mussatto S I, Fernandes M, Rocha G J M, et al. Production, characterization and application of activated carbon from brewer›s spent grain lignin[J]. Bioresource Technology, 2010, 101(7): 2450-2457. PBM